Low-loss dielectric-loaded graphene surface plasmon polariton waveguide based biochemical sensor

Thamani M. Wijesinghe,[1] Malin Premaratne,[1,a)] and Govind P. Agrawal[2]
[1]*Advanced Computing and Simulation Laboratory (AχL), Department of Electrical and Computer Systems Engineering, Monash University, Clayton, Victoria 3800, Australia*
[2]*Institute of Optics, University of Rochester, Rochester, New York 14627, USA*

(Received 22 February 2015; accepted 25 May 2015; published online 5 June 2015)

We have modeled and numerically simulated the performance of a dielectric-loaded graphene surface-plasmon-polariton (DL-GSPP) waveguide as a biochemical sensing device. In our device, the conventionally used gold layer is replaced with a graphene microribbon for the detection of biochemical molecules. The graphene layer is incorporated to minimize ohmic losses and to enhance the adsorption of biomolecules so that the sensor sensitivity is increased significantly. The sensor performance is quantified through numerical simulations carried out by varying device parameters such as waveguide length, effective mode index, dimension of the dielectric ridge, and the length and the number of graphene layers. One of the prominent features of our DL-GSPP waveguide sensor is that its length is in the millimeter range, an essential requirement for realistic plasmonic waveguide sensors. The average sensitivity of DL-GSPP structure is found to be in the range of 3–6 μRIU (refractive index units), which is comparable to the values obtained using surface-plasmon resonance (1–10 μRIU) and long-range waveguide sensors (0.1–5 μRIU). [http://dx.doi.org/10.1063/1.4922124]

I. INTRODUCTION

Plasmonics has attracted significant attention over the past few decades, owing to the revolutionary impacts that it has on both the fundamental physics and practical applications in various disciplines.[1–3] As surface-plasmon-polariton (SPP) modes are laterally confined on a sub-wavelength scale, plasmonics have been employed to realize many efficient nano/micro devices.[1,2] As one of the first commercial applications of plasmonic techniques, SPPs are used to build biological and chemical sensors with greater sensitivity compared to conventional sensing methods.[3] Biosensors are used in the fields of drug discovery, medical diagnosis, and detection of harmful pathogens. The sensing material responds selectively to biological targets (or analytes) via a specific molecular recognition probe and converts this biological recognition event into a sensing signal via a proper transducer based on optical, thermal, or electrochemical effects.[4–6] The analyte molecules can be antibodies, enzymes, proteins, immunosystems, tissues, organelles, or whole cells.[6] The commonly used bioreceptors are DNA molecules, aptamers, antibodies, ligand, enzymes, microorganism, cells, and tissues.[6]

Surface-plasmon resonance (SPR) biosensors use SPPs to probe the interaction between analyte molecules and the sensor surface. Since SPPs are extremely sensitive to changes in the dielectric constant at the surface, even a relatively small change in the molecular density on the sensor surface can be detected accurately. For this reason, SPPs are often used for improving the resolution of chemical and biological sensors through a technique called label-free sensing.[3,6] Typically, SPR sensors based on prism coupling have resolution in the range of 1–10 μRIU (refractive index units).[7,8] Efforts are being made to improve biosensors so that they are in the form of compact portable devices that can be used for rapid and high-throughput measurements of analytes to provide real-time information. This can be achieved by using proper materials with new device architectures.[6] In this context, SPP waveguides are of considerable interest. A metal–dielectric waveguide structure supports SPPs that can be used to probe biological substances by measuring the mode amplitude, with a resolution around 0.5–1 μRIU.[9–12] To improve the performance further, several different SPP waveguide configurations have been considered in recent years.[13–18] But most of them do not have long enough propagation length to be practical as a biosensor. The longer propagation length and larger sensing depth of long-range SPPs (LRSPPs) provide a larger interaction length and enhance adlayer sensitivity.[19] Essentially, these contribute to lower the detection limit and increase the overall sensitivity of the sensor. Several SPP waveguide designs have been proposed to balance the trade-off between the field confinement and propagation length.[18,20–22] The dielectric-loaded SPP (DLSPP) waveguide employs a dielectric ridge on top of the metal substrate that confines the mode to the dielectric region and leads to longer propagation lengths compared to the strip, slot, and grove configurations.[18,23,24]

In this paper, we consider graphene, a one-atom-thick platform for infrared and terahertz (THz) metamaterials, which can support surface electromagnetic waves.[25] A monolayer of graphene with very low chemical potential behaves like a semiconductor and supports guiding of a transverse-electric (TE)-polarization SPPs.[26] If graphene is

a)malin.premaratne@monash.edu

highly doped, it behaves like a thin metal film and allows for the guiding of transverse-magnetic (TM)-polarization SPPs. Similar to a thin metal stripe that supports low-loss, LRSPP stripe modes, graphene microribbons can guide long-range graphene SPP (LR-GSPP) stripe modes. Such modes exhibit an average extinction ratio of 19 dB at a wavelength of 1.31 μm and have been used successfully in experiments for data transmission at a bit rate of 2.5 Gb/s.[27–29] The devices fabricated with metals suffer from large Ohmic losses and cannot be tuned once the geometry of the structure is fixed. In sharp contrast, electronic properties of graphene can be tuned via electrical gating or chemical doping. Graphene's electronic sensitivity to biomolecular adsorption on its surface has also been studied for many applications.[30–34] It is found that graphene can adsorb biochemical molecules more efficiently than gold.[35] In this paper, we demonstrate that a dielectric-loaded graphene SPP (DL-GSPP) waveguide can be exploited as a sensing device. We discuss in Sec. II the guiding properties of a DL-GSPP waveguide and calculate the effective refractive index of its modes. In Sec. III, we employ the waveguide as a biosensor and calculate its sensitivity. The main results and major findings of our study are summarized in Sec. IV.

II. DL-GSPP WAVEGUIDE

Graphene, a flat monolayer of carbon atoms packed into a dense two-dimensional honeycomb crystal lattice, has the merits of a small effective electron mass, high carrier mobility, and strong interaction with light over a broad frequency range.[25] The conductivity of graphene can be modified by means of chemical doping, electric fields, or magnetic fields. Additionally, when the interband optical transition dominates and the imaginary part of graphene conductivity is negative, graphene can support a TM-polarized SPP mode, a feature that has enormous potential for plasmonic waveguide applications.[26,36]

Graphene is described by a surface conductivity σ_g, which is related to the radiation frequency ω, temperature T, electron relaxation time τ, and chemical potential (Fermi level, E_f). The intraband and interband conductivity of the monolayer graphene can be calculated from the Kubo formula in the limit $E_f \gg k_B T$, where k_B is the Boltzmann constant[36]

$$\sigma_{intra} = \frac{iq^2}{\pi\hbar^2}\frac{E_f}{(\omega + i\tau^{-1})}, \tag{1}$$

$$\sigma_{inter} = \frac{q^2}{4\hbar}\left[1 + \frac{i}{\pi}\ln\frac{\hbar(\omega + i\tau^{-1}) - 2E_f}{\hbar(\omega + i\tau^{-1}) + 2E_f}\right]. \tag{2}$$

The total conductivity, $\sigma_{g,2D} = \sigma_{intra} + \sigma_{inter}$, is related to the in-plane permittivity as

$$\varepsilon_g \approx 1 + \frac{i\sigma_{g,2D}}{\varepsilon_0 \omega t_g}, \tag{3}$$

where t_g is the thickness of the graphene microribbon. Different from conventional metals, the Fermi level of graphene is tunable by applying an electric field or by doping it to with p-type or n-type materials. Thus, we can control the graphene's carrier density and the rate of interband transitions (via excitation of electron-hole pairs). Figure 1 shows how the real and imaginary parts of the permittivity ($\varepsilon_g = \varepsilon_g' + i\varepsilon_g''$) and the refractive index ($n = n_g + i\kappa_g$) vary with the Fermi energy of graphene. Throughout this study, we assume a fixed operating wavelength, $\lambda = 1.55\,\mu$m. At $E_f = 0.4$ eV, ε_g' and n_g attain their peak values, while ε_g'' and κ_g take their minimum values. Given that SPPs can only be excited in a metal–dielectric interface, metallic interface must be present in the waveguide configuration. We achieve this by manipulating the Fermi potential of graphene. As clearly depicted in Fig. 1, for values over $E_f = 0.6$ eV, κ_g increases and n_g decreases, showing transition from dielectric to metallic characteristics of graphene, suitable to sustaining SPPs on a graphene interface.

Figure 2 shows how a dielectric-loaded graphene microribbon based waveguide structure can be used for sensing applications. The waveguide configuration includes a low-index substrate ($n = 1.34$), a SiO_2 buffer layer ($n = 1.45$), a graphene microribbon, a polymer ridge ($n = 1.535$), and a microfluidic medium ($n = 1.33$).

To find the SPP modes supported by the structure shown in Fig. 2, we need to solve the Helmholtz equation satisfied by the electric field

$$\nabla^2\mathbf{E} + (k_0^2\varepsilon_r - \beta^2)\mathbf{E} = 0, \tag{4}$$

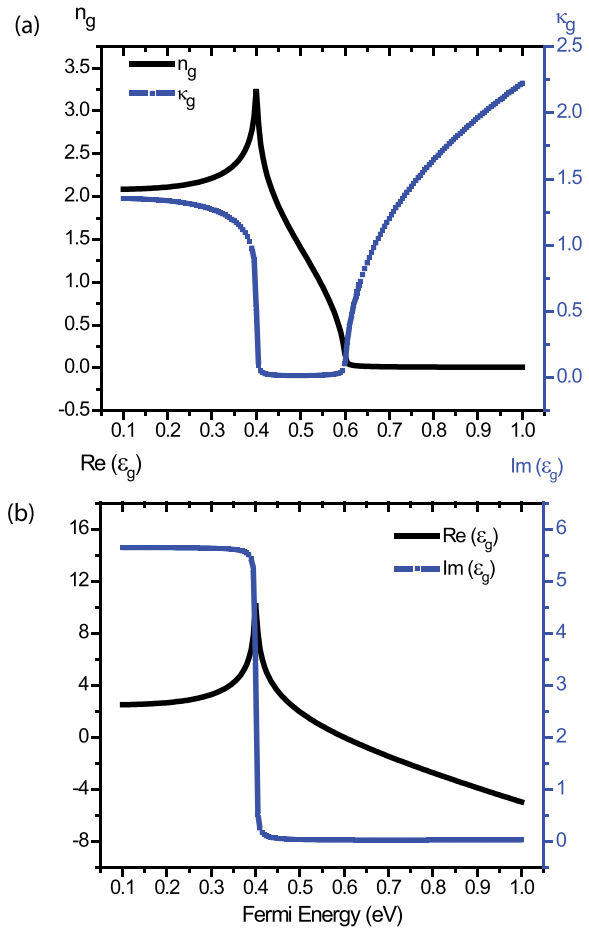

FIG. 1. Variation of the real and imaginary parts of the (a) permittivity and (b) refractive index with the Fermi energy of a monolayer of graphene. We consider $\lambda = 1.55\,\mu$m in this study.

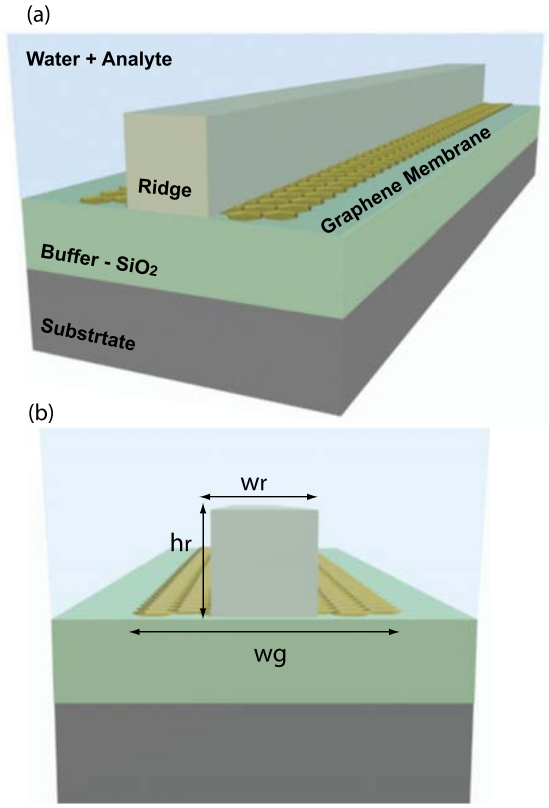

FIG. 2. (a) The configuration of DL-GSPP waveguide nanostructure with (b) the dimension parameters of the cross section.

where β is in-plane complex propagation constant of the SPP mode along, $k_0 = \omega/c$ is the vacuum wave number, and ε_r is the relative permittivity of each material. The magnetic and electric field components of the fundamental SPP mode (TM_{00}) are $\mathbf{H} = H_x$ and $\mathbf{E} = E_y$, E_z, respectively.[37] Obtaining an analytical solution for our two-dimensional complex structure is comparatively challenging. Therefore, numerical techniques must be used to find accurate solutions. In our study, a numerical solver based on the finite-element method (FEM) was used to calculate the modes.[38]

Figure 3(a) shows how the real and imaginary parts of the effective index ($n_{eff} = \beta/k_0$) of the SPP mode vary with E_f. Both of them have peaks at 0.4 and 0.6 eV. The propagation length of the SPP mode is calculated from $L_{spp} = \frac{1}{2}\mathrm{Im}(n_{eff})$. Figure 3(b) shows how L_{spp} varies with E_f. The SPP mode dominates when graphene behaves as a metal. This is the reason why L_{spp} increases significantly after $E_f = 0.6$ eV. If we consider a thin layer of gold instead of graphene, the minimum practical thickness is 15 nm. Then, L_{spp} that can be achieved is only around 60 μm at $\lambda = 1.55$ μm. In contrast, it can be increased to 16 mm when a monolayer of graphene is used in place of gold. The millimeter length scale is sufficient to measure the output power and mode amplitude for sensing techniques.

It is possible to study variations of mode effective index and L_{spp} with the height h_r and width w_r of the ridge. We consider h_r in the range of 0.5–1.2 μm and w_r in the range of 0.5–1.4 μm and assume that the width and thickness of the graphene microribbon are $w_g = 1.4$ μm and $t_g = 1$ nm, respectively. We set Fermi energy at $E_f = 0.7$ eV to obtain a large

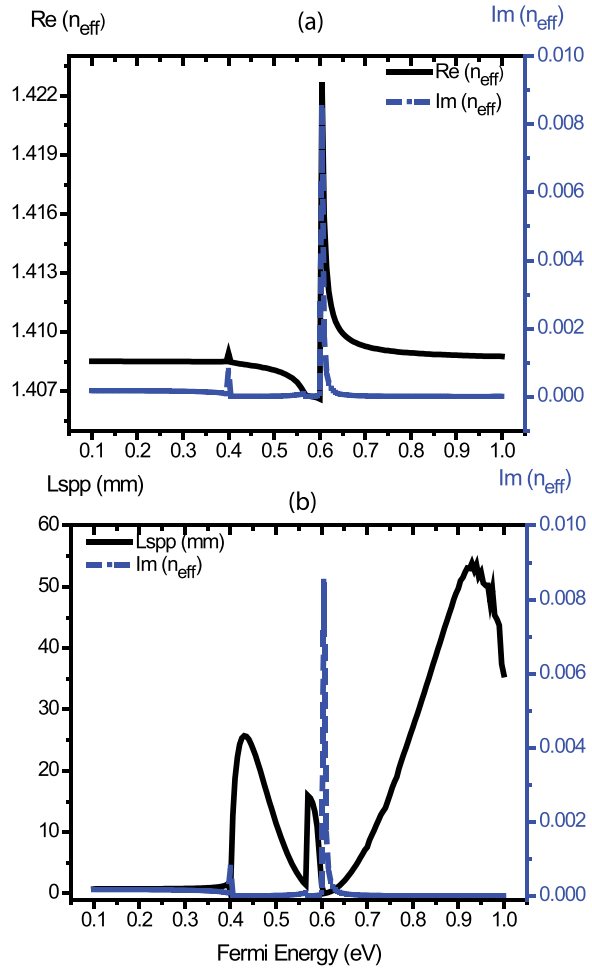

FIG. 3. Variations with the Fermi energy of graphene of the (a) real and imaginary components of the effective mode index and (b) propagation length of the SPP mode.

SPP mode area and to avoid high intrinsic losses (with increased κ_g). Figure 4 shows our numerical results as a comparison with gold. In Fig. 4(a), $\mathrm{Re}(n_{eff})$ is increasing with h_r and w_r and reaches a maximum value of 1.43 for $h_r = 1.2$ μm and $w_r = 1.4$ μm. In Fig. 4(b), $\mathrm{Im}(n_{eff})$ is relatively small in the region of $w_r > 1.0$ μm and $0.5 < h_r < 0.8$ μm. This leads to a maximum value of about 16 mm for L_{spp} as in Fig. 4(c). This behavior can be understood from Figs. 5(a)–5(c) where the mode profiles (magnetic field and electric field) in the structure are shown for three different combinations of w_r and h_r. In general, there is a trade-off between mode confinement and propagation length. When there is a high mode confinement, it increases losses too. However, when h_r is reduced, the mode spreads across the graphene layer into the low-index buffer and substrate regions, which reduces mode losses drastically and increases the propagation length. If a thin metal layer is used instead of graphene, the mode will not spread in such way [refer Fig. 5(a)]. Mode leaking into cladding and buffer region is an advantage in sensing applications, as it increases the mode interaction depth with the analyte while maintaining the long propagation length.

The minimum thickness of a metal film (e.g., gold) that can be commercially fabricated is around 10–15 nm and κ_g is higher when compared to graphene at the same frequency.

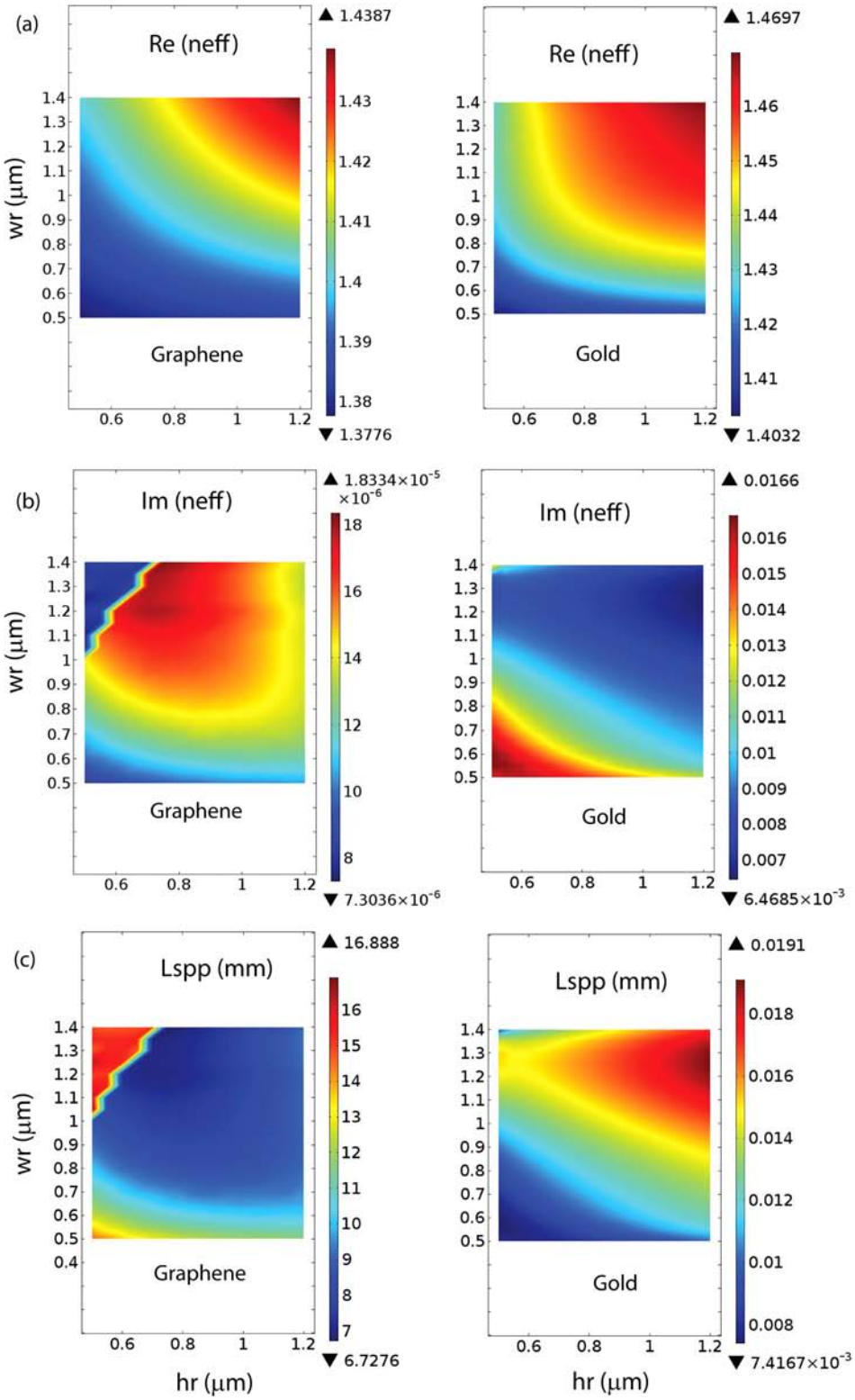

FIG. 4. The variations of (a) real and (b) imaginary parts of effective mode index and (c) propagation length with the width w_r and height h_r of the ridge. Left panel for graphene and right panel for gold layer. $w_g = 1.4\,\mu$m, $t_g = 1$ nm, $E_f = 0.7$ eV, and $\lambda = 1.55\,\mu$m.

Owing to this, excited mode experiences high intrinsic losses. Compared to graphene, gold has a very high Im(n_{eff}), that drastically reduces the mode propagation length. Further reduction of gold stripe thickness (<15 nm) will hardly lead to a significant decrease propagation-loss in practice due to fabrication difficulties in creating a very thin homogeneous metal layer.[39] Some studies have shown that proper SPP waveguiding was not observed for the thinnest gold films.[40] Further, surface flatness of thin metal films also influenced by the roughness of cladding/substrate surface.[39] There are limitations for fabrication of homogenous ultra-thin metal films using industrial fabrication techniques such as large scale uv-lithography and lift-off process conditions.[16,41] Thus, graphene is a viable low-loss alternative to gold thin film as graphene waveguides inherit all of the advantages and unique features of graphene such as high adsorption efficiency, electrochemical tunability, mode confinement, low losses, and crystalline structure.

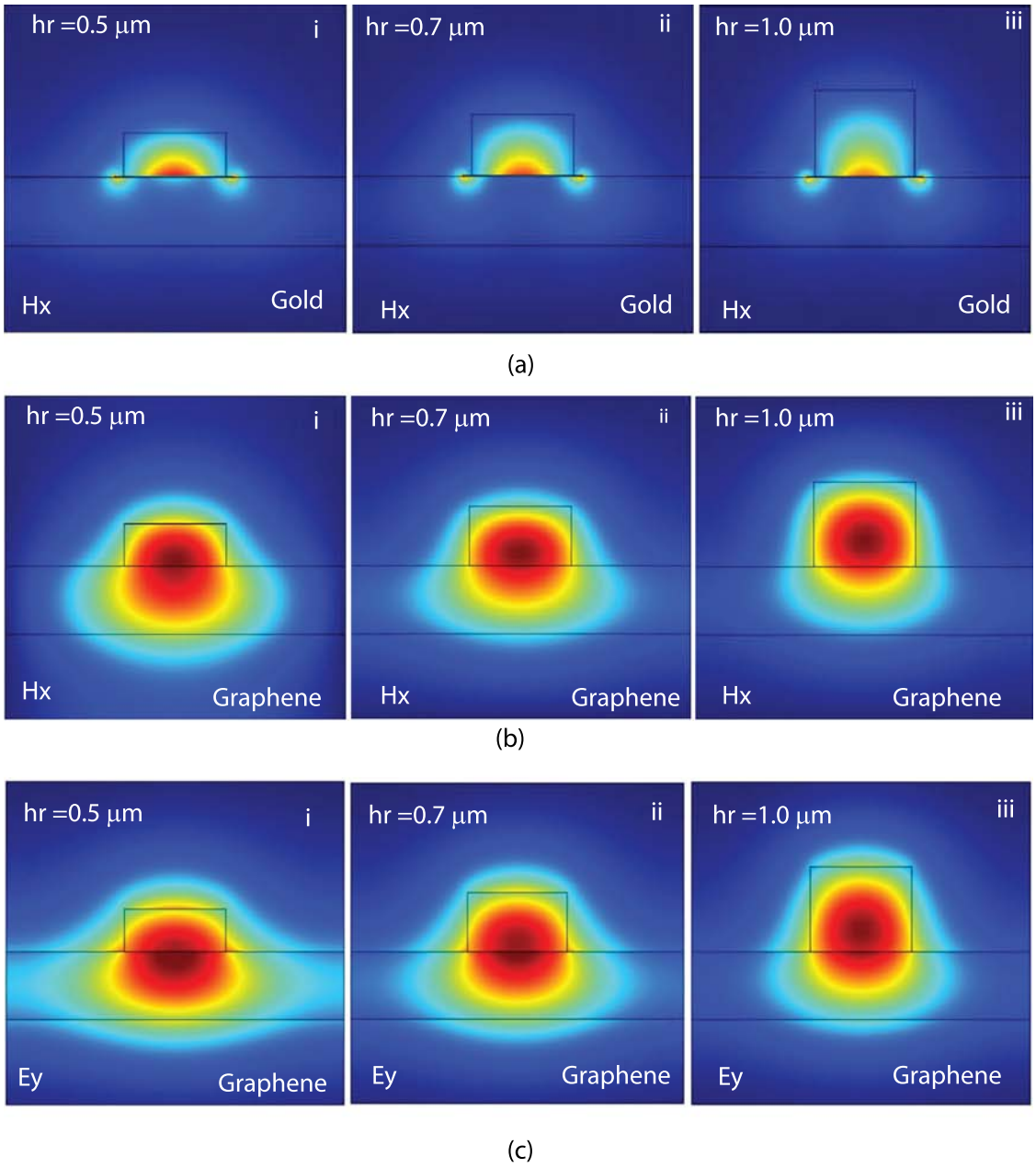

FIG. 5. (a) The H_x component for gold, (b) H_x component and (c) E_y component for graphene, for $h_r = 0.5, 0.7, 1.0\,\mu$m. $w_r = 1.2\,\mu$m, $w_g = 1.4\,\mu$m, $t_g = 1$ nm, $E_f = 0.7$ eV, and $\lambda = 1.55\,\mu$m.

III. OUTPUT POWER AND SENSITIVITY

The SPP mode is highly sensitive to the permittivity distribution in the plasmonic structure. Even relatively small changes in the permittivities of various materials can drastically change the effective index, amplitude, power, and propagation length of the SPP mode. Power measurements are commonly used as a sensing technique to probe analyte in the microfluidic medium. In this section, we investigate the sensing performance of the proposed structure by considering refractometric measurements of the output power. Borrowing from optical waveguide theory, the output power P_{out} is related to the input powers P_{in} as[42]

$$P_{\text{out}} = P_{\text{in}} \exp(-2\beta'' L_s) = P_{\text{in}} \exp(-L_s/L_{\text{spp}}), \qquad (5)$$

where we used the fact that the imaginary part of β is related inversely to the SPP length L_{spp}.

Presence of a substance (such as moles of biomolecules—ΔM) in the microfluidic medium perturbs fluid's refractive index by an amount of Δn. The sensitivity (s_M) of the sensing device depends on changes in the output power (ΔP) in response to these changes and is defined as[43]

$$s_M^P = \frac{\Delta P}{\Delta M} = \frac{\Delta P}{\Delta n} \cdot \frac{\Delta n}{\Delta M}. \qquad (6)$$

Noting that $E_d = \Delta n/\Delta M$ is the adsorption efficiency of the target molecule and defining sensitivity to refractive index change as $s_n^P = \Delta P/\Delta n$,[34,42,43] we obtain the simple relation

$$s_M^P = s_n^P E_d, \qquad (7)$$

where s_n^P is in units of W/RIU.

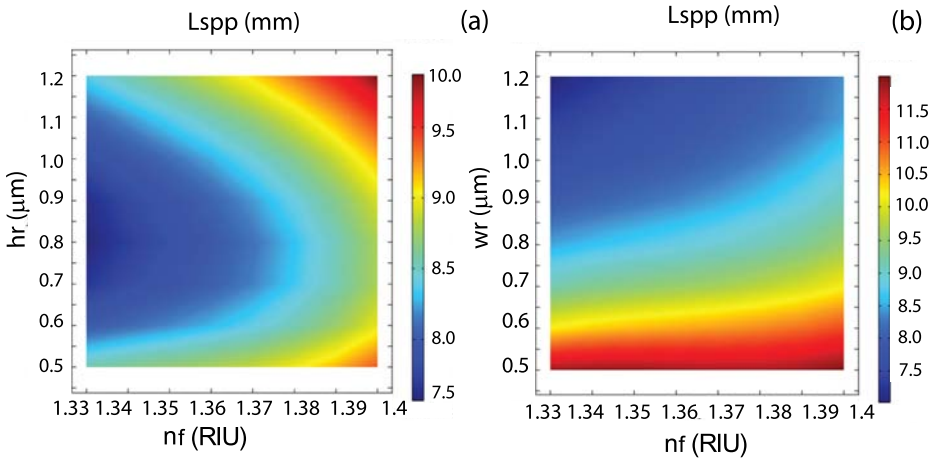

FIG. 6. The variation of mode propagation length with (a) h_r and n_f for $w_r = 1.0\,\mu$m and (b) w_r and n_f for $h_r = 0.8\,\mu$m. The thickness and width of graphene membrane remain the same ($w_g = 1.4\,\mu$m and $t_g = 1$ nm) and $P_{in} = 1$ W.

Another important parameter of the sensor is Limit of Detection (LOD) for homogenous sensing, which is defined as the minimum detectable refractive index change of the analyte solution. The LOD is inversely proportional to the refractive index sensitivity, s_n^P.[44] Owing to this dependency, to improve the performance of the device, it is usually desired to increase s_n^P and decrease LOD as far as possible. The LOD can be calculated as the ratio of the minimum detectable signal of the power probe, δp, to the refractive index sensitivity, s_n^P (Ref. 45)

$$LOD = \frac{1}{s_n^P} \times \delta p = \left(\frac{\Delta P}{\Delta n}\right)^{-1} \delta p. \tag{8}$$

LOD defines in RIU. Since ΔP is a function of L_s, it can be maximized by operating the device near $\frac{dP}{dL_s} \to 0$. This relation defines the optimum value for L_s that leads to maximum output power variations in terms of the perturbed and unperturbed L_{spp} values[42]

$$L_{opt} = \frac{L_{spp}L'_{spp}}{L'_{spp} - L_{spp}} \ln\left(\frac{L'_{spp}}{L_{spp}}\right). \tag{9}$$

To illustrate the sensitivity of our proposed device, we assume that the presence of a specific analyte substance changes the refractive index of the microfluid in the range of 1.33–1.4. Figures 6(a) and 6(b) show variations of L_{spp} with h_r and w_r in the given range of n_f. When $w_r = 1.0\,\mu$m, for the values of h_r in the range of 0.5–1.2 mm, L_{spp} varies from 7.5 to 10 mm and increases with n_f. For the values of w_r varying from 0.5 to 1.2 mm with $h_r = 0.8\,\mu$m, L_{spp} varies from 6.9 to 12 mm and decreases with w_r. According to Eq. (9), L_{opt} falls in between this range for each n_f value, which decides the length of waveguide, L_s, to obtained maximum sensitivity. Figures 7(a) and 7(b) illustrate variations of normalized output power ($P_n = P_{out}/P_{in}$) and sensitivity (s) with h_r, and Figs. 8(a) and 8(b) illustrate the same with w_r. P_n gradually increases with n_f for all values of h_r, showing a minimum power level for $h_r = 0.8\,\mu$m. Similarly, P_n gradually increases with n_f for all values of w_r, and power level is reduced with increasing w_r, with a maximum for $w_r = 0.5\,\mu$m. As seen in Figs. 7(b) and 8(b), the sensitivity varies in between 0.25–1.1 W/RIU and 0.1–1.0 W/RIU for the two cases. If we assume the resolution of power probe is 0.0004%,[42] for $s_n^P = 0.6$ W/RIU as an average value, LOD can approach the value of 6.67 μRIU.

Figure 9(a) illustrates how the propagation length of SPP mode varies with n_f when width w_g of the graphene microribbon varies in the range of 1.0–1.6 μm. As seen there, L_{spp} gradually increases with n_f but it decreases with w_g. In these simulations, values of w_r, h_r, and E_f are fixed as 1 μm, 0.8 μm, and 0.7 eV, respectively. Figure 9(b) depicts variations of normalized output power and exhibits a trend similar to that observed for L_{spp}. As shown in Fig. 9(c), sensitivity is

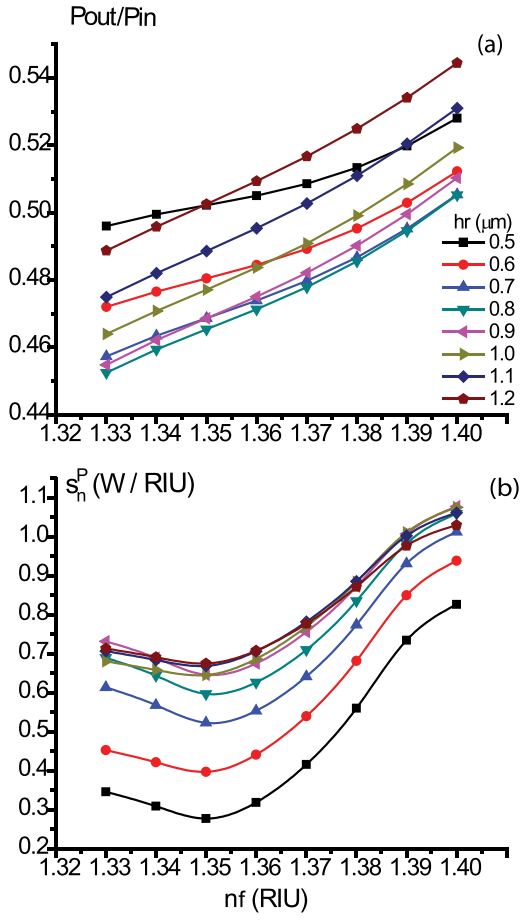

FIG. 7. The variation of (a) normalized output power and (b) sensitivity with h_r and n_f for $w_r = 1.0\,\mu$m. $w_g = 1.4\,\mu$m and $t_g = 1$ nm and $P_{in} = 1$ W.

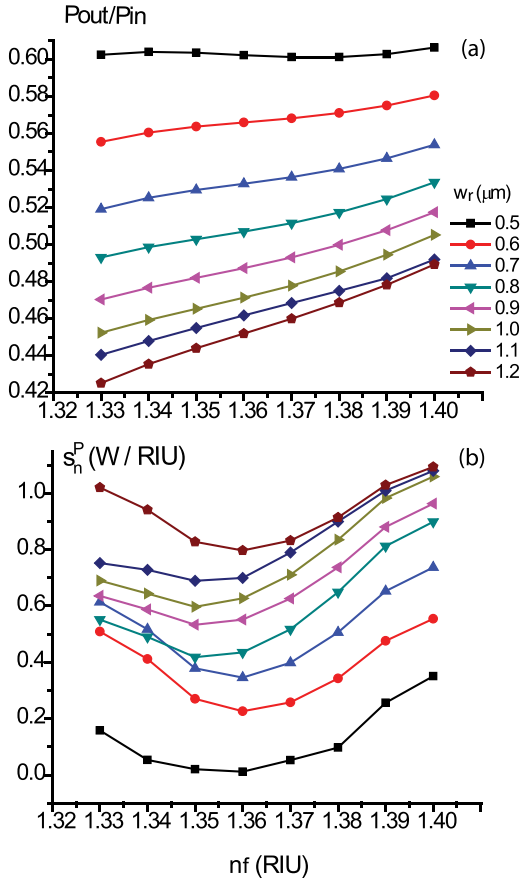

FIG. 8. The variations of (a) normalized output power and (b) sensitivity with w_r and n_f for $h_r = 0.8\ \mu$m. $w_g = 1.4\ \mu$m and $t_g = 1$ nm and $P_{in} = 1$ W.

the lowest for n_f around 1.36. If we assume values $w_g = 1.2\ \mu$m and $n_f = 1.34$, LOD can be take the value of 3.6 μRIU. The waveguide structure has a low-index dielectric buffer and substrate with refractive indices 1.45 and 1.34, respectively. The lower sensitivity around analyte-index 1.35 can be seen due to the symmetry around buffer layer leading to high mode confinement. That slightly lowers the output power and the sensitivity in the range 1.34–1.36.

Thickness of the graphene microribbon can be changed by adding more graphene layers. In the THz range, the optical conductivity of graphene is approximately proportional to the number of layer N, i.e., $\sigma_N = N\sigma_{mono}$.[46] Figures 10(a) and 10(b) show variations in the normalised output power and sensitivity with n_f when N is increased from 1 to 6. Sensitivity goes down when increasing the number of layers. The graphene microribbon with two layers gives average sensitivity values, $s_n^P = 0.9\ \mathrm{W/RIU}$ and $\mathrm{LOD} = 4.45\ \mu$RIU for $n_f = 1.39$.

IV. DISCUSSION AND CONCLUSIONS

In this paper, we focused on designing a graphene-based SPP waveguide as an efficient sensing device in the THz regime. Our proposed dielectric-loaded SPP waveguide helps to realize a graphene-assisted biological sensor whose ridge configuration makes it relatively easy to integrate the SPP waveguide with the microfluidic system. Since the propagation length of the SPP mode can be maximized at the

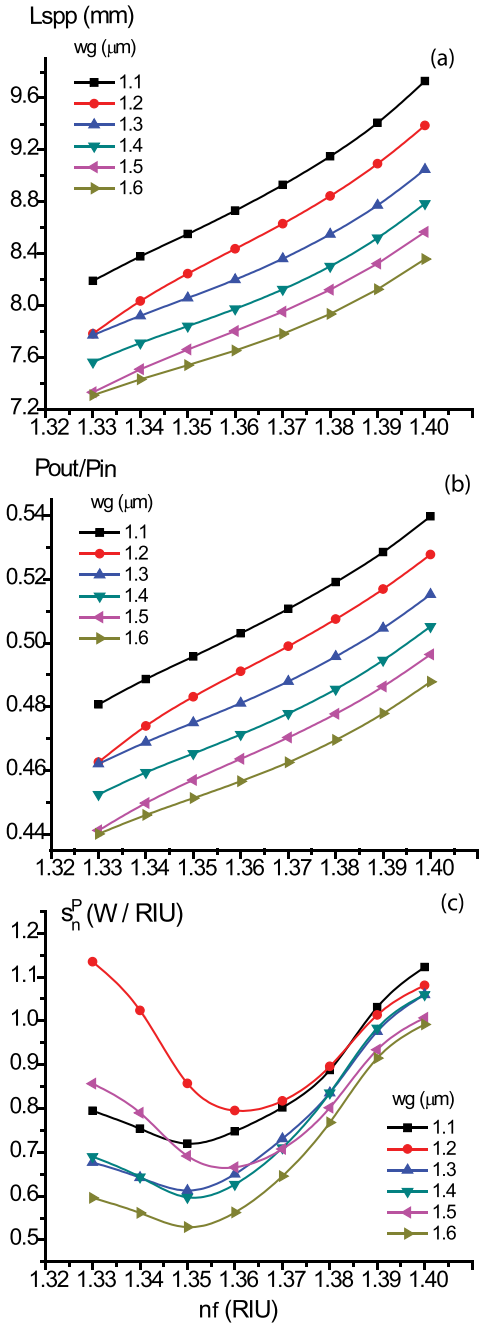

FIG. 9. (a) Variations of mode propagation length with the width of the graphene microribbon for different Fermi energies. Variations of (b) normalized output power and (c) sensitivity with n_f for different widths of graphene microribbon. Assumed parameter values were $w_r = 1\ \mu$m, $h_r = 0.8\ \mu$m, and $E_f = 0.7$ eV.

interface between the graphene and the ridge, sensitivity of such a biosensor can be greatly enhanced. Proposed DL-GSPP waveguide has a cross section area of $4 \times 4\ \mu\mathrm{m}^2$ with a maximum ridge height of 1.4 μm for a 1.6 μm width of the graphene microribbon. As shown in Fig. 1, doped graphene with the Fermi energy of 0.7 eV leads to metallic properties with less lossy conditions compared to noble metals.

The performance of the device is assessed in terms of propagation length, mode index (confinement), output power, and sensitivity under different design conditions, including dimensions of the dielectric ridge, length of the

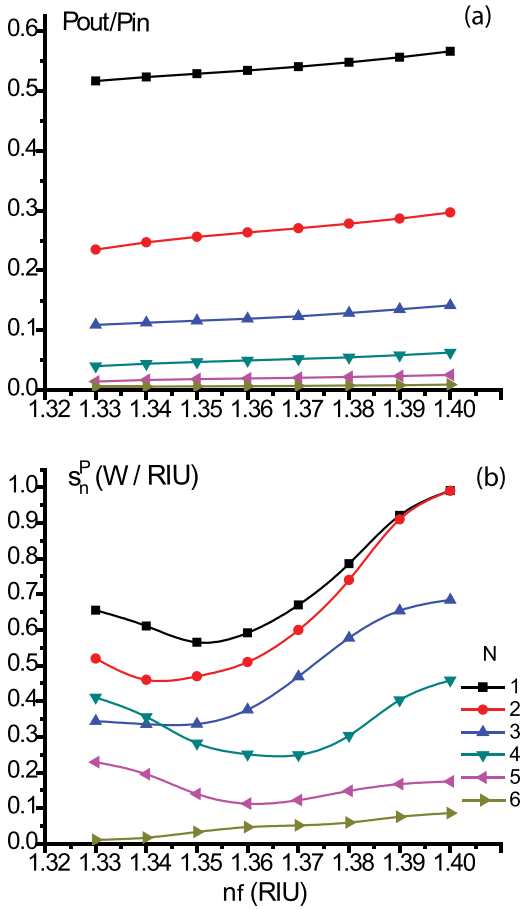

FIG. 10. Variations of (a) normalized output power and (b) sensitivity with n_f for different number of graphene layers. Assumed the following parameter values: $w_r = 1\ \mu$m, $h_r = 0.8\ \mu$m, $w_g = 1.4\ \mu$m, and $E_f = 0.7$ eV.

graphene microribbon, and number of graphene layers. One of the prominent features of our DL-GSPP waveguide sensor is that its length is in the millimeter range, an essential requirement for realistic palsmonic waveguide sensors. The average LOD of DL-GSPP structure is found to be in the range of 3–6 μRIU, which is comparable to the values obtained using surface-plasmon resonance (1–10 μRIU) and long-range waveguide sensors (0.1–5 μRIU).[3–6,11,12]

Placing a thin metal stripe with the graphene layer can increase the detection limit towards 0.1 μRIU, but it also drastically reduces the SPP propagation length (below 100 nm). To avoid high losses and to keep dimensions closer to sub-wavelength scale, metal elements are not included in this design. This is not a problem since graphene adsorbs biomolecules (e.g., ssDNA, RNA, glycans, proteins, and peptides) more strongly and stably compared to the gold surface.[6] Such adhesion and differentiation properties suggest that a graphene microribbon is an excellent bio-compatible material compared to a metal.[35] The adsorption efficiency is expected to be greater for graphene compared to gold ($E_g > E_{Au}$), but it has to be confirmed experimentally. Therefore, sensitivity is expected to increase significantly than the previous theoretically reported values.[34,47] In the case of biomolecules, the refractive index variation occurs mainly in the sensor surface, therefore defining a detection thickness (an adlayer shown in Fig. 11(a)), h_d in the range of 1–600 nm is more appropriate and significantly accurate for sensitivity calculations. Figure 11(b) depicts the variation of sensitivity with n_f and h_r for $h_d = 200$ nm. Figure 11(c) illustrates the variation of sensitivity with the thickness of adlayer having a refractive index of 1.34. Sensitivity improves non-linearly with the adlayer thickness varying up to 650 nm.

In the proposed structure, TM-polarized SPP mode is possible to excite in an end-fire/butt-coupled arrangement. The optical source of the waveguide sensor can be designed as a CW-tunable diode laser having $P_{in} = 10$ mW, and coupled easily to the incident port. The high coupling efficiency of both input and output ports can be achieved with a taper-shape dielectric waveguide converter.[48,49] A high resolution power-meter (e.g., $\delta p < 0.0005\%$) can be used to detect the propagated signal of the waveguide sensor.[42] In

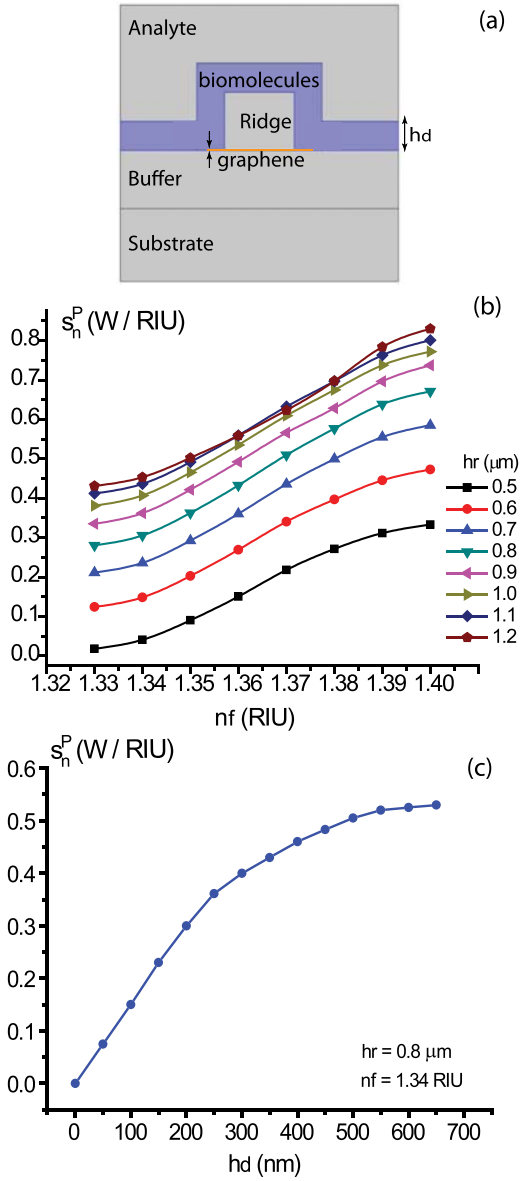

FIG. 11. (a) The adlayer thickness h_d illustrated on the sensor surface. (b) The variation of sensitivity with n_f and h_r for $w_r = 1.0\ \mu$m and $h_d = 200$ nm. (c) The variation of sensitivity with adlayer thickness for $h_r = 0.8\ \mu$m, $w_r = 1.0\ \mu$m, and $n_f = 1.34$ RIU.

addition, for the better agreement with the theoretical modelling, a noise minimising technique must be required in the experimental set up. For the substrate, we chose a low-index material to confine the mode into the ridge area; however, additional use of silicon substrate may be required in order to be compatible with the standard microelectronic fabrication technology.[11] Graphene film can be grown by thermal chemical vapor deposition (CVD) method. The Fermi level of graphene can be tuned through surface transfer doping or substitutional/impurity doping by using appropriately selected set of dopants.[50,51] Graphene plasmons are being experimentally investigated in many occasions.[52,53] The THz and far-infrared SPP in graphene microribbons has been recently observed.[27,28] Apart from sensitivity, selectivity is probably the most important feature of a biosensor. Selectivity means that sensor detects a certain analyte and does not react to admixtures and contaminants.[6] Antigen-antibody interaction is considered to have the highest selectivity in a biosensor. Investigation of non-uniformity of adlayer, effect of bio-receptors, and calculating selectivity coefficients for the proposed DL-GSPP sensor will be addressed in the next stage of our research, considering an analyte-specific experimental approach.[54]

In conclusion, the proposed DL-GSPP waveguide is a potential structure to develop efficient plasmonic sensing devices. Millimeter-range propagation lengths and high adsorption of molecules due to graphene microribbon should lead to improve waveguide sensors compared to other conventional structures. The analysis and discussion presented here should prove valuable for developing an efficient, high-precision, biochemical sensing technique.

ACKNOWLEDGMENTS

The authors thank Monash University Institute of Graduate Research (MIGR) for the financial support. The work of M. Premaratne and G. P. Agrawal was supported by the Australian Research Council through its Discovery Grant Scheme under Grant No. DP140100883.

[1]S. Lal, S. Link, and N. Halas, Nat. Photonics **1**, 641–648 (2007).
[2]W. L. Barnes, A. Dereux, and T. W. Ebbesen, Nature **424**, 824–830 (2003).
[3]J. Homola, S. Yee, and G. Gauglitz, Sens. Actuators, B **54**, 3–15 (1999).
[4]R. Harris and J. Wilkinson, Sens. Actuators, B **29**, 261–267 (1995).
[5]J. Dostálek, Sens. Actuators, B **76**, 8–12 (2001).
[6]J. Li and N. Wu, *Biosensors Based on Nanomaterials and Nanodevices* (CRC, 2013).
[7]F. Liu, Y. Rao, Y. Huang, D. Ohnishi, W. Zhang, and J. Peng, in *Proceedings of International Symposium on Biophotonics, Nanophotonics and Metamaterials* (2006), pp. 103–105.
[8]F. Chien and S. Chen, Biosens. Bioelectron. **20**, 633–642 (2004).
[9]R. Charbonneau, M. Tencer, N. Lahoud, and P. Berini, Sens. Actuators, B **134**, 455–461 (2008).
[10]D. Handapangoda, I. D. Rukhlenko, M. Premaratne, and C. Jagadish, Opt. Lett. **35**, 4190–4192 (2010).
[11]O. Krupin, H. Asiri, C. Wang, R. Tait, and P. Berini, Opt. Express **21**, 698–709 (2013).
[12]Y. Li, A. Ma, L. Yang, and X. Zhang, Plasmonics **9**, 71–78 (2014).
[13]Y. Huang, P. Dastmalchi, and G. Veronis, in Quantum Electronics and Laser Science Conference (2014), p. 89880.
[14]A. Babu, C. Bhagyaraj, J. Jacob, G. Mathew, and V. Mathew, Opt. Quantum Electron. **45**, 481–490 (2013).
[15]M. Kwon, Plasmonics **5**, 347–354 (2010).
[16]N. Fong, P. Berini, and R. Tait, Proc. SPIE 89151F (2013).
[17]Y. Joo, S. Song, D. Ussery, K. Lee, and R. Magnusson, in *Frontiers in Optics* (2009), p. JWC44.
[18]P. Karasinski, R. Rogozinski, and A. Opilski, Proc. SPIE 218–222 (2001).
[19]Y. Joo, S. Song, and R. Magnusson, Opt. Express **17**, 10606–10611 (2009).
[20]T. Holmgaard and S. Bozhevolnyi, Phys. Rev. B **75**, 245405 (2007).
[21]R. Oulton, V. Sorger, D. Genov, D. Pile, and X. Zhang, Nat. Photonics **2**, 496–500 (2008).
[22]D. Pile and D. Gramotnev, Opt. Lett. **29**, 1069–1071 (2004).
[23]A. Krasavin and A. Zayats, Appl. Phys. Lett. **90**, 211101 (2007).
[24]A. Pannipitiya, I. D. Rukhlenko, and M. Premaratne, IEEE Photonics J. **3**, 220–233 (2011).
[25]A. Neto, F. Guinea, N. Peres, K. Novoselov, and A. Geim, Rev. Mod. Phys. **81**, 109–162 (2009).
[26]K. Ooi, H. Chu, L. Ang, and P. Bai, J. Opt. Soc. Am. B **30**, 3111–3116 (2003).
[27]J. Kim, H. Choi, Y. Yu, K. Chung, and C. Choi, Proc. SPIE 898802 (2014).
[28]J. Kim and S. Choi, Opt. Express **19**, 24557–24562 (2011).
[29]X. He and S. Kim, J. Opt. Soc. Am. B **30**, 2461–2468 (2013).
[30]M. Pumera, Mater. Today **14**, 308–315 (2011).
[31]S. Szunerits, N. Maalouli, E. Wijaya, J. Vilcot, and R. Boukherroub, Anal. Bioanal. Chem. **405**, 1435–1443 (2013).
[32]M. Artiles, C. Rout, and T. Fisher, Adv. Drug Delivery Rev. **63**, 1352–1360 (2011).
[33]P. Jahanshahi and F. Adikan, J. Med. Biol. Eng. **4**, 145–149 (2015).
[34]L. Wu, H. S. Chu, W. Koh, and E. P. Li, Opt. Express **18**, 14395–14400 (2010).
[35]B. Song, D. Li, W. Qi, M. Elstner, C. Fan, and H. Fang, ChemPhysChem **11**, 585–589 (2010).
[36]J. Gosciniak and D. Tan, Nanotechnology **24**, 185202 (2013).
[37]S. A. Maier, *Plasmonics: Fundamentals and Applications* (Springer-Verlag, Berlin, 2007).
[38]T. Wijesinghe, M. Premaratne, and G. Agrawal, Opt. Express **22**, 185202 (2014).
[39]V. Shalaev and S. Kawata, *Nanophotonics with Surface Plasmons* (Elsevier, 2006).
[40]I. Slovinsky, G. Stefansson, A. Kossoy, and K. Leosson, Plasmonics **8**, 1613–1619 (2013).
[41]Y. Xie, T. Liu, X. Zhao, M. Zhang, C. Chen, F. Wang, and D. Zhang, J. Opt. **16**, 065006 (2014).
[42]G. Magno, M. Grande, V. Petruzzelli, and A. D'Orazio, Sens. Actuators, B **186**, 148–155 (2013).
[43]P. Berini, New J. Phys. **10**, 105010 (2008).
[44]A. Sun and Z. Wu, Sensors **12**, 7318–7325 (2012).
[45]I. M. White and X. Fan, Opt. Express **16**, 1020–1028 (2008).
[46]I. T. Lin, "Optical properties of graphene from the THz to the visible spectral region" MSc thesis (University of California, Los Angeles, 2012).
[47]M. Islam, A. Kouzani, X. Dai, W. Michalski, and H. Gholamhosseini, J. Biomed. Nanotechnol. **8**, 380–393 (2012).
[48]F. Liu, R. Wan, Y. Li, Y. Huang, Y. Miura, D. Ohnishi, and J. Peng, Appl. Phys. Lett. **95**, 091104 (2009).
[49]X. Li, L. Huang, Q. Tan, B. Bai, and G. Jin, Opt. Express **19**, 6541–6548 (2011).
[50]H. Liu, Y. Liu, and D. Zhu, J. Mater. Chem. **21**, 3335–3345 (2010).
[51]J. Kim, H. Choi, Y. Yu, K. Chung, and C. Choi, in *Integrated Optics: Devices, Materials, and Technologies XVIII* (2014), p. 898802.
[52]N. Papasimakis, Z. Luo, Z. X. Shen, F. D. Angelis, E. D. Fabrizio, A. E. Nikolaenko, and N. I. Zheludev, Opt. Express **18**, 8353–8359 (2010).
[53]L. Ju, B. Geng, J. Horng, C. Girit, M. Martin, Z. Hao, and F. Wang, Nat. Nanotechnol. **6**, 630–634 (2011).
[54]Y. Shao, J. Wang, H. Wu, J. Liu, I. Aksay, and Y. Lin, Electroanalysis **22**, 1027–1036 (2010).